Vanessa Werth*, Kai Volgmann, Mazharul M. Islam,
Paul Heitjans and Thomas Bredow

Density Functional Theory Evaluated for Structural and Electronic Properties of 1T-Li_xTiS_2 and Lithium Ion Migration in 1T-$Li_{0.94}TiS_2$

DOI 10.1515/zpch-2016-0919
Received October 18, 2016; accepted March 7, 2017

Abstract: In many applications it has been found that the standard generalized gradient approximation (GGA) does not accurately describe weak chemical bond and electronic properties of solids containing transition metals. In this work, we have considered the intercalation material 1T-Li_xTiS_2 ($0 \le x \le 1$) as a model system for the evaluation of the accuracy of GGA and corrected GGA with reference to the availabile experimental data. The influence of two different dispersion corrections (D3 and D-TS) and an on-site Coulomb repulsion term (GGA + U) on the calculated structural and electronic properties is tested. All calculations are based on the Perdew-Burke-Ernzerhof (PBE) functional. An effective U value of 3.5 eV is used for titanium. The deviation of the calculated lattice parameter c for TiS_2 from experiment is reduced from 14 % with standard PBE to –2 % with PBE + U and Grimme's D3 dispersion correction. 1T-TiS_2 has a metallic ground state at PBE level whereas PBE + U predicts an indirect gap of 0.19 eV in agreement with experiment. The ^7Li chemical shift and quadrupole coupling constants are in reasonable agreement with the experimental data only for PBE + U-D3. An activation energy of 0.4 eV is calculated with PBE + U-D3 for lithium migration via a tetrahedral interstitial site. This result is closer to experimental values than the migration barriers previously obtained at LDA level. The proposed method PBE + U-D3 gives a reasonable description of structural and electronic properties of 1T-Li_xTiS_2 in the whole range $0 \le x \le 1$.

***Corresponding author: Vanessa Werth,** Institut für Physikalische Chemie und Elektrochemie, Leibniz Universität Hannover, Callinstr. 3-3a, 30167 Hannover, Germany, e-mail: vanessa.werth@pci.uni-hannover.de
Kai Volgmann and Paul Heitjans: Institut für Physikalische Chemie und Elektrochemie, Leibniz Universität Hannover, Callinstr. 3-3a, 30167 Hannover, Germany; and Zentrum für Festkörperchemie und Neue Materialien (ZFM), Leibniz Universität Hannover, Callinstr. 3-3a, 30167 Hannover, Germany
Mazharul M. Islam and Thomas Bredow: Mulliken Center for Theoretical Chemistry, Institut für Physikalische und Theoretische Chemie, Universität Bonn, Beringstr. 4, 53115 Bonn, Germany

Keywords: band structure; chemical shift; DFT + U; dispersion correction; Li ion diffusion; lithium titanium disulfide; migration barrier; quadrupole coupling constant.

1 Introduction

Rechargeable lithium ion batteries are commercially used for more than 20 years [1]. Research in the field of lithium ion batteries goes even back forty years, when Whittingham investigated layered TiS_2 as a cathode material [2]. Since then the suitability of various phases of TiS_2 as cathode materials have been studied many times both experimentally and theoretically. The most frequently studied phase is 1T-TiS_2 [2–19] which crystallizes in the CdI_2 structure (space group $P\bar{3}m1$) and consists of titanium disulfide layers parallel to the *ab* plane. The layers have an AB stacking sequence and are connected mainly by van der Waals forces. Therefore various guest atoms can be intercalated between these layers, either at the octahedral position (Wyckoff site 1*b*) or at the tetrahedral 2*d* position [3, 8]. In the case of lithium, the octahedral position is energetically preferred. No phase transition has been observed for 1T-Li_xTiS_2 within $0 \le x \le 1$ at ambient temperature. Formally one Ti^{4+} is reduced to Ti^{3+} for each intercalated Li (assuming full charge transfer), which generates one unpaired electron per Li atom. The extra electron is inserted into the TiS_2 conduction band [20] which results in a metallic diamagnetic behavior at room temperature and a paramagnetic behavior at temperatures below 100 K [21].

A large number of theoretical and experimental studies were performed to understand the lithium ion diffusion process in 1T-Li_xTiS_2 [9, 10, 16, 18, 22, 23]. Migration barriers for the diffusion process have been determined experimentally via nuclear magnetic resonance (NMR) techniques and theoretically at density-functional theory (DFT) level. For $x \approx 1$, the composition considered in this study regarding lithium ion migration, the experimentally determined migration barriers are 0.26 and 0.48 eV [22, 23], 0.31 eV [9] and 0.24 eV [10]. These values were obtained with different NMR methods and therefore do not necessarily describe the same migration process (see, e.g. refs. [24–26]). Previously calculated activation barriers obtained for local migration processes via a tetrahedral site (pathway 1*b*→2*d*→1*b*′ where 1*b*′ is initially empty) are 0.70 eV and 0.42 eV [16], depending on the occupation of surrounding 1*b* sites. In the theoretical study of Islam and Bredow an activation barrier of 0.75 eV was determined for the hopping mechanism to a tetrahedral position without lithium vacancy [18]. In the latter study direct diffusion via the center of a sulfur octahedron edge connecting 1*b* and 1*b*′ was also studied. The corresponding activation energies ranged from 0.45 to 0.49 eV [18].

The accurate description of structural properties of 1T-Li_xTiS_2 in the whole range of $0 \le x \le 1$ represents a challenge for available theoretical methods. With standard DFT methods, the calculated lattice parameters – in particular the *c* lattice parameter – for $x \to 0$ [27–29] strongly deviate from experimental values [4]. This is mainly due to the local description of electron correlation with generalized gradient approximation (GGA) DFT which does not account for nonlocal effects such as London dispersion. A coincidental error cancelation occurs for local density approximation (LDA) calculations [16]. This deficiency of standard DFT has been remedied in the last years. Besides nonlocal vdW-DF [30], basically two versions of dispersion correction are used in modern applications, either the D3 method by Grimme et al. [31, 32], or the D-TS method by Tkatchenko and Scheffler [33]. For $x \to 1$, the London dispersion effects are not significant as the interaction between the TiS_2 layers and intercalated Li^+ is predominantly electrostatic.

A second problem is the accurate theoretical description of the electronic structure of 1T-Li_xTiS_2. For $x \to 0$, the system is a semiconductor while for larger *x* it becomes metallic at room temperature [20]. Due to the self-interaction error, the standard GGA-DFT methods tend to underestimate experimental electronic band gaps and artificially delocalize unpaired electrons. This problem is reduced by Hartree-Fock DFT hybrid methods with a certain contribution of Hartree-Fock exchange in the exchange functional. However, the calculation of Hartree-Fock exchange is computationally demanding using plane-wave methods. Therefore simpler correction schemes such as LDA + U or GGA + U have been developed [34]. In the most simple form of GGA + U, an on-site Coulomb repulsion term is added to the Kohn-Sham matrix elements of *d* and *f* atomic orbitals. Recently the GGA + U method was applied to study Li ion conductors [28, 29, 35–39].

In the present work the effect of the GGA + U method and the D3 dispersion correction on calculated structural properties of 1T-TiS_2 and 1T-$LiTiS_2$ is studied. Their effect on electronic properties and NMR parameters (quadrupole coupling constant and chemical shift) of 1T-$LiTiS_2$ and on the activation barriers for 1T-Li_xTiS_2 (with $x \approx 1$) is also evaluated.

2 Computational details

All calculations are performed with the plane-wave program package VASP [40–43]. The projector-augmented wave (PAW) method is used for the core electron representation [44, 45]. The *s* and *p* semicore states are treated as valence states for Ti. For sulfur the standard version of the PAW potential is used. After convergence tests, we have used a cutoff energy $E_{cut} = 600$ eV. A Γ-centered $6 \times 6 \times 3$

Monkhorst-Pack (MP) *k*-point grid is used for reciprocal space sampling [46]. With these settings, the total energy/cell is converged within 0.001 eV. Smaller MP grids are employed for the supercell calculations. NMR parameters are calculated with a $12\times12\times6$ MP grid and a cutoff of 1200 eV. Additionally an all-electron PAW for lithium is used for these calculations. The reference for the chemical shift is crystalline LiCl where the shift is calculated for the optimized lattice parameter, 1200 eV cutoff energy and $8\times8\times8$ MP grid.

The underlying standard GGA functional employed in this study is PBE [47, 48]. PBE energies are corrected for London dispersion effects by the DFT-D3 method [31, 32] and the D-TS approach [33]. The DFT + U method (with $U-J=U_{\mathrm{eff}}$) introduced by Dudarev [34] is applied to the *d* orbitals of Ti. The U_{eff} value is optimized to fit the energy difference between diamagnetic and ferromagnetic spin structures of 1T-$LiTiS_2$ obtained with the hybrid functional HSE06 [49] (with the same accuracy parameters as described above). At 0 K, the ground state has been found to be paramagnetic [21]. As the paramagnetic spin state with randomly distributed atomic spin vectors would require extremely large supercells, usually a ferromagnetic or a simplified antiferromagnetic spin state is used as an approximation. Using PBE without corrections, the diamagnetic (DM) closed-shell state is more stable than the ferromagnetic (FM) spin state. This is checked using the accurate tetrahedron method with Blöchl corrections [50]. With HSE06, which is considered to provide a more accurate account of open-shell transition metal compounds [51], the FM state is 0.2 eV more stable than the DM state. With DFT + U (where $U_{\mathrm{eff}}=3.5$ eV) this energy difference is reproduced.

Activation barriers for Li ion migration are calculated with the CI-NEB method [52, 53] employing a $Li_{17}Ti_{18}S_{36}$ supercell which corresponds to the composition $Li_{0.94}TiS_2$. Full frequency calculations were performed in order to verify the saddle point character of the images with highest energy.

3 Experimental activation barriers

A careful comparison with experimental results is crucial for any theoretical work. This is especially important in the field of ion migration processes in solids. Experimentally activation barriers for ion migration can be obtained with macroscopic and microscopic methods [54, 55]. These cover short and long range transport phenomena at different extents. Therefore the numerical values of the obtained barriers may differ significantly.

With the CI-NEB method, energy barriers for local atomic jump processes are calculated. Comparison of these barriers should therefore be restricted to experimental methods that also describe microscopic processes, e.g. solid-state nuclear

magnetic resonance (NMR) spectroscopy. NMR measurements can be performed with various techniques which may provide different activation barriers [24–26].

Diffusion-induced peaks of NMR spin-lattice relaxation (SLR) rates both in the laboratory (T_1^{-1}) and the rotating ($T_{1\rho}^{-1}$) frame of reference, plotted on a logarithmic scale vs. reciprocal temperature have a high-temperature and a low-temperature flank. In the work [23] a figure containing the results of T_1^{-1} and $T_{1\rho}^{-1}$ measurements for 1T-$LiTiS_2$ can be found. Each slope results in an activation barrier Q_{high} and Q_{low}, respectively. For 1T-$LiTiS_2$ Q_{high} turns out to be 0.31(1) eV and Q_{low} is 0.27 eV for both types of measurements. For the isotropic case and uncorrelated jumps, these barriers are expected to be equal. 1T-$LiTiS_2$ is a two-dimensional ion conductor and therefore Q_{high} is influenced by the dimensionality effect. Non-random, i.e. correlated jumps, would influence Q_{low} due to Coulomb interactions or structural disorder.

At the maxima of the T_1^{-1} and $T_{1\rho}^{-1}$ relaxation rates, the conditions $\omega_0\tau_c \approx 1$ and $\omega_1\tau_c \approx 0.5$ hold where ω_0 and ω_1 denote the respective Larmor frequency. From these maxima, the motional correlation times τ_c can be calculated which are in the same order of magnitude as the mean residence time τ. If Larmor frequency and jump rate τ_c^{-1} are equal, one single atomic jump is 'seen' within the time window of a Larmor precession period. In this way, the jump rates are determined essentially independent of a specific diffusion model, solely from the frequency dependent positions of the relaxation rate maxima $T_{1,max}^{-1}$ and $T_{1\rho,max}^{-1}$ on the temperature scale [56]. The reciprocal values of τ_c often show an Arrhenius behavior and an activation barrier Q_{max} can be estimated in this way. A straight line connecting the jump rates taken from the maxima of the T_1^{-1} and $T_{1\rho}^{-1}$ peaks yields an activation barrier Q_{max} of 0.48 eV. This result is only presented in the PhD thesis of Wilkening [22], but can be reproduced using the results in [23].

For comparison with CI-NEB calculations the activation barrier Q_{max} resulting from the Arrhenius plot of the rate maxima is used. This value represents one atomic jump, being largely independent of details of the diffusion process, as it is the case in CI-NEB calculations.

4 Results

4.1 Structure of 1T-$LiTiS_2$ and 1T-TiS_2

First we have performed an evaluation of selected dispersion corrections and combinations with on-site U correction in terms of the accuracy of structural parameters of $LiTiS_2$ and TiS_2. For these two compounds, which represent the extreme

cases of high ($x=1$) and low ($x=0$) Li contents, experimental reference data are available [4]. The differences between the calculated values of the most critical *c* lattice parameter from the experimental data are shown in Figure 1. Deviations for the *a* lattice parameter are generally smaller and less method dependent. As expected, PBE without dispersion correction strongly overestimates the *c* lattice parameter of TiS_2. On the other hand, the *c* lattice parameter of $LiTiS_2$ agrees well with the experimental data. The interaction is mainly of electrostatic nature. Augmenting the PBE functional with a dispersion correction improves the overall description of both structures, but leads to an underestimation of the TiS_2 *c* lattice parameter. PBE+U combined with dispersion correction results in an improvement of the obtained lattice parameters. Differences between D3 and D-TS are about 1 % for $LiTiS_2$ and negligible for TiS_2. If PBE+U is used without dispersion correction, the deviation from experiment increases. In general, the *c* lattice parameter is smaller for the FM state compared to the DM state.

The unmodified PBE method provides accurate lattice parameters for 1T-$LiTiS_2$ but strongly deviates for $x \ll 1$. Thus it cannot be used in studies of the whole intercalation range. Additionally the magnetic ground state obtained with PBE is DM which is not correct at 0 K.

The best results for structural and electronic properties are obtained with the PBE+U-D3 method. The differences between D-TS and D3 are small but D3 provides slightly better agreement with the experimental data. Therefore the D3 method is used for all subsequent calculations.

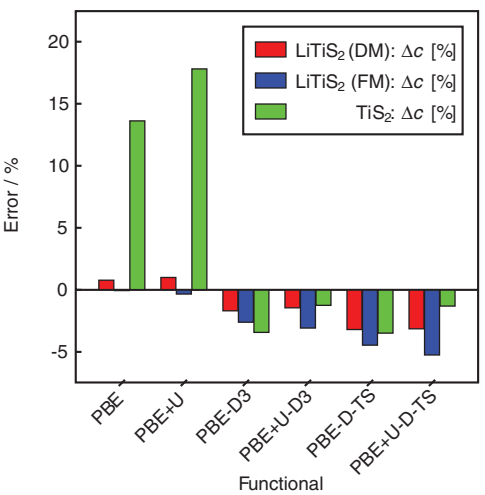

Fig. 1: Deviations of calculated *c* lattice parameters from experimental values (in percent) for diamagnetic $LiTiS_2$ (red), ferromagnetic $LiTiS_2$ (blue) and TiS_2 (green).

4.2 Band structure

The band gap of TiS_2 was investigated many times both experimentally [57–65] and theoretically [5, 11, 66–74]. Experimental studies suggest that TiS_2 is a semiconductor with a small indirect band gap between 0.18 eV [63] and 0.56 eV [65]. Theoretically there is still an ongoing debate whether TiS_2 is a semiconductor with a small gap or a semimetal. In this study, we have calculated the band structure of TiS_2 with PBE, PBE + U and the hybrid method HSE06 assuming experimental lattice parameters [75]. The HSE06 calculations were performed with a $6 \times 6 \times 6$ MP grid and a cutoff of 600 eV (the same as for PBE and PBE + U) and the same energy convergence criteria. The resulting band structures are given in Figure 2.

The unmodified PBE method predicts a metallic ground state for TiS_2. With PBE + U an indirect band gap of 0.19 eV is obtained which is in good agreement with experimental data. The HSE06 calculation yields an indirect gap of 0.55 eV. The general shapes of the bands obtained with these three methods are similar. The indirect band gap predicted by PBE + U and HSE06 results from a sulfur *p* band at Γ and a titanium *d* band at *L*. A direct band gap of 0.76 eV (PBE + U) and 1.15 eV (HSE06), respectively, is obtained at the Γ point.

Typically the U_{eff} value is optimized to fit the experimental gap or the one obtained from high quality calculations (e.g. hybrid or quasi-particle calculations). We would like to state that, in the present case, the optimization of U_{eff} value to the FM-DM energy difference obtained with a hybrid method leads to a band gap in good agreement with experiment. The indirect band gaps obtained with both PBE + U and HSE06 are within the experimental range of 0.18–0.56 eV.

4.3 NMR parameters for ^{7}Li of 1T-$LiTiS_2$

Activation energies obtained from the CI-NEB calculations are compared with values obtained by NMR experiments. As an additional test, we have also compared the calculated NMR parameters with experimental data. Experimental quadrupole coupling constants C_q were taken from the work of Bredow et al. [14] and chemical shifts $\Delta\delta(^7\text{Li})$ from the PhD thesis of Küchler [76]. A comparison between theory and experiment is given in Tables 1 and 2.

The calculations are performed for both DM and FM states in order to investigate the effect of the spin state on magnetic properties. For 1T-Li_xTiS_2 with $x = 1.0$ PBE overestimates the experimental value by ≈15 kHz in the DM state, and by ≈8 kHz in the FM state. The deviations obtained with PBE + U-D3 are slightly smaller, ≈ + 8 kHz (DM) and ≈ – 6 kHz (FM). For $x = 0.7$ and $x = 0.3$ the measured C_q

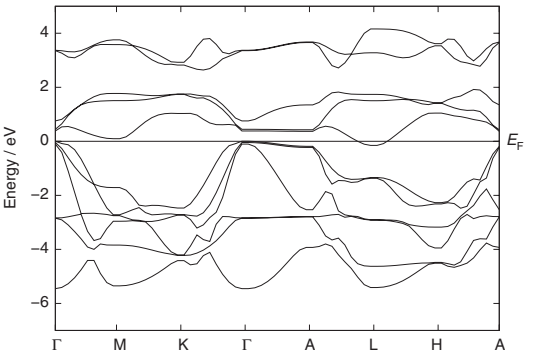

(a) TiS_2 band strucure from PBE.

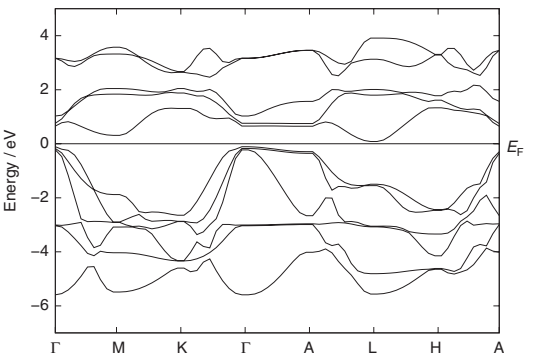

(b) TiS_2 band strucure from PBE+U.

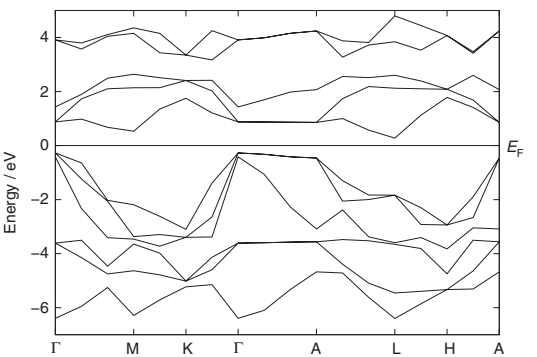

(C) TiS_2 band strucure from HSE06.

Fig. 2: TiS_2 band structures for the experimental geometry calculated with (a) PBE, (b) PBE + U (U_{eff} = 3.5 eV) and (c) the hybrid method HSE06. PBE exhibit semimetallic behavior with an overlap of a sulfur *p* band and a titanium *d* band. PBE + U and HSE06 represent semiconducting behavior with an indirect band gap between the Γ and *L* point. PBE + U result in an indirect gap of 0.19 eV and HSE06 of 0.55 eV.

Tab. 1: Quadrupole coupling constants $C_q(^7Li)$ calculated for different magnetic states, different functionals and different lithium amounts.

Method	x in Li_xTiS_2	$C_q(^7Li)$/kHz
PBE (DM)	1.00	47
	0.67	44
	0.33	37
PBE (FM)	1.00	39
	0.67	39
	0.33	36
PBE + U-D3 (DM)	1.00	39
	0.67	30
	0.33	18
PBE + U-D3 (FM)	1.00	25
	0.67	14
	0.33	13
Exp. [14]		
$T = 158$ K	1.0	31 ± 2
$T = 373$ K	0.7	14.8 ± 0.5
$T = 143$ K	0.7	11 ± 2
$T = 373$ K	0.3	<5

The calculations were performed with optimized lattice parameters and atomic positions.

Tab. 2: Chemical shift $\Delta\delta$ with reference to LiCl calculated for different magnetic states, different functionals and $x = 1$.

Method	$\Delta\delta(^7Li)$/ppm
PBE (DM)	27.1
PBE (FM)	25.2
PBE + U-D3 (DM)	11.5
PBE + U-D3 (FM)	26.5
Exp. [76]	2.5

The calculations were performed with optimized lattice parameters and atomic positions.

decreases by 16–20 kHz and by more than 26 kHz with respect to $x = 1.0$, respectively. This trend is best reproduced with PBE + U-D3 in the DM state. C_q decreases by 9 kHz ($x = 0.7$) and 21 kHz ($x = 0.3$), respectively, The corresponding changes in the FM state are –11 kHz and –12 kHz. The effect of Li content is much less pronounced with uncorrected PBE. C_q changes by –3 kHz and –10 kHz (DM state) and by 0 kHz and –3 kHz (FM state), respectively, for $x = 0.7$ and 0.3 compared to $x = 1.0$. Thus the overall agreement of calculated quadrupole coupling constants with experiment is improved by the U and D3 corrections.

The calculations for the chemical shift $\Delta\delta(^7\text{Li})$ are performed with the fully optimized structures. The reference material for the theoretical calculations was crystalline LiCl whereas in experiments the shift was measured with respect to a 1 M LiCl solution. The difference between those two states is however only –1.1 ppm [77] and therefore the introduced error is small.

The experimental shift for 1T-$LiTiS_2$ is 2.5 ppm [76]. Closest agreement is achieved with PBE + U-D3 (DM) which overestimates this value by 9 ppm. All other methods result in deviations larger than 20 ppm.

The chemical shift obtained with PBE + U-D3 in the DM state is in much better agreement than the corresponding result for the FM state ($\Delta = +24$ ppm). This is reasonable as these measurements are performed above 100 K where the material is diamagnetic.

4.4 Li ion migration in $Li_{0.94}TiS_2$

In 1T-Li_xTiS_2 Li ion migration from an octahedral 1*b* site to a neighboring empty 1*b*′ site can occur via two different pathways (Figure 3). The first pathway is accomplished via the interstitial tetrahedral (Tet) site (1*b*→2*d*→1*b*′). This pathway was proposed for $Li_{0.7}TiS_2$ by Wilkening and Heitjans [56]. The second possibility is a direct migration via the center of the sulfur octahedron edge connecting 1*b* and

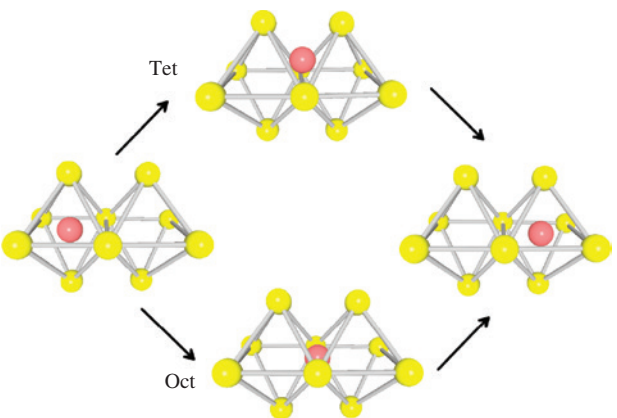

Fig. 3: For the octahedrally coordinated lithium ion (pink) there are two possible migration pathways to reach the nearest vacant octahedral site.
Tet – interstitial mechanism: migration occurs via tetrahedral position 2*d*.
Oct – direct pathway: Migration takes place via the sulfur (yellow) octahedron edge connecting the lithium ion position with the vacancy.

1*b*′ (Oct). This migration pathway was considered for $Li_{0.88}TiS_2$ in a previous study of Islam and Bredow [18].

Since our calculations show that a tetrahedral site is not a local minimum for lithium in $Li_{1.0}TiS_2$, we started the Li migration calculation by introducing one Li vacancy in our model, a $3\times3\times2$ supercell ($Li_{17}Ti_{18}S_{36}$ corresponding to $Li_{0.94}TiS_2$). Since the deviation from $x=1$ is small, we expect the obtained migration barrier to be comparable to experimental values obtained for $Li_{1.0}TiS_2$. Larger supercells are required to further increase x towards 1.0. This however strongly increases the computational costs and was not possible with available computer resources. Since the distance between equivalent Li sites is 10.5 Å in the $3\times3\times2$ supercell, we assume that defect-defect interactions are negligible.

The Oct minimum energy pathway (MEP) is shown in Figure 4. The energy maximum (image 2) corresponds to a structure where the migrating Li is located in the center between two sulfur atoms as shown in Figure 3. For PBE (solid lines), the MEP is almost unaffected by the spin state. In contrast, the energy curves for PBE+U-D3 show a pronounced difference between the DM and FM states. For the DM state the maximum energy of PBE+U-D3 is lower than PBE by ~0.1 eV. The FM state shows the opposite behavior. However, frequency calculations of the maximum energy structures reveal that the obtained structures for image 2 are not transition states. Two imaginary frequencies are obtained and therefore

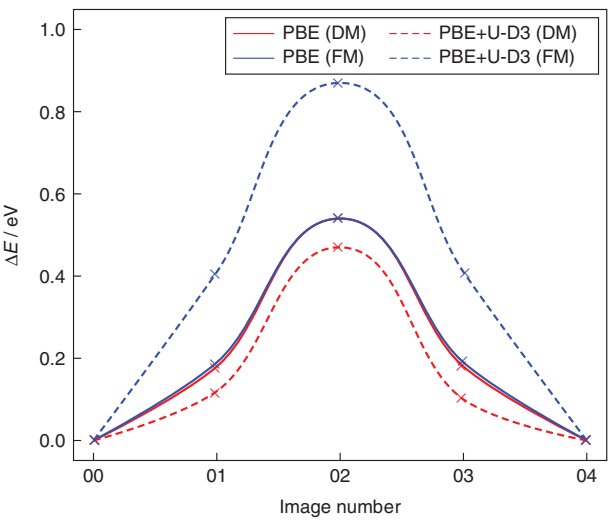

Fig. 4: Minimum energy pathway for the Oct migration obtained from the CI-NEB method with three images. The pathway is calculated with PBE (solid lines) and PBE+U-D3 (dashed lines) for FM (blue) and DM (red) spin states.

this migration pathway will not be considered any further. Thus – in contrast to considerations of previous studies [18] – the present results indicate that a direct migration pathway is not likely for $x \approx 1$.

The Tet MEP is shown in Figure 5. The energy maximum arises from the position of the lithium ion in the center of a sulfur octahedron face which is shared by the Tet site. The MEP curves for the different methods show a similar behavior as for the Oct MEP. The activation energy obtained with PBE + U-D3 in the DM state (0.40 eV) is significantly lower than in the FM state (0.64 eV), but only slightly lower than the barriers calculated with PBE (0.45 eV in the DM state and 0.42 eV in the FM state, see table 3). Frequency calculations confirm the transition state nature of all obtained maximum energy structures. The higher barrier obtained

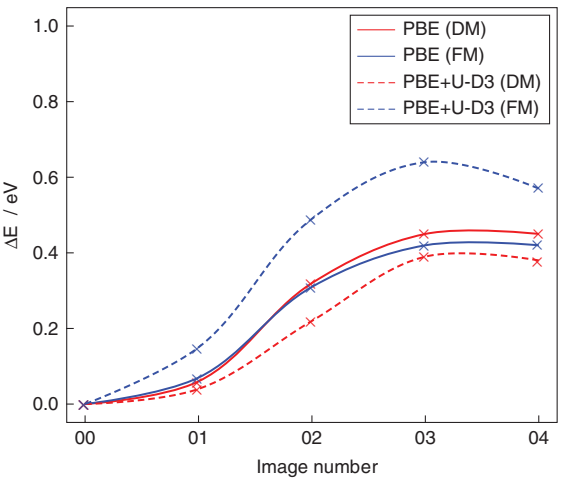

Fig. 5: Minimum energy pathway for the Tet migration obtained from the CI-NEB method with three images for lithium ion migration from the octahedral to the tetrahedral position. Each pathway is calculated with PBE (solid lines) and PBE + U-D3BJ (dashed lines) for FM (blue) and DM (red) spin states.

Tab. 3: The activation energies obtained for the Tet migration with the different methods for $Li_{0.94}TiS_2$.

Method	E_A/eV
PBE (DM)	0.45
PBE (FM)	0.42
PBE + U-D3 (DM)	0.40
PBE + U-D3 (FM)	0.64

with PBE + U-D3 in the FM state is a result from a spin transfer between neighboring Ti atoms during the CI-NEB calculation which will not be observed in experiments at room temperature due to the diamagnetic nature of $LiTiS_2$ under these conditions.

Van der Ven et al. [16] calculated a considerably larger barrier of 0.7 eV for the Tet migration pathway at LDA level. This method provides reasonable structure parameters for $LiTiS_2$ similar to PBE. However, it is well known that LDA tends towards overbinding which could explain the larger barrier.

In section 3 'Experimental activation barriers', we have given a detailed explanation regarding the choice of the experimental barrier for comparison with theory. The barrier $Q_{max} = 0.48$ eV obtained from the maxima of the T_1^{-1} and $T_{1\rho}^{-1}$ peaks, provided in [23], is chosen for comparison, as these maxima represent a single atomic jump. This closely resembles the model calculations performed here with the CI-NEB method. With PBE + U-D3 in a DM state this barrier is underestimated by 0.08 eV. Also the activation barriers obtained with PBE are in agreement with this value. The good agreement obtained with PBE is partly due to the good structural description of Li_xTiS_2 with $x \approx 1$. For lower lithium contents the results obtained with PBE may not be satisfying as the large deviation in the *c* lattice parameter will greatly influence the activation energy for the migration process.

5 Summary

Structural, electronic and spectroscopic properties of $LiTiS_2$ with various lithium amounts were studied with PBE and PBE + U approaches using dispersion corrections D3 and D-TS. The structural properties for $LiTiS_2$ are well described with every tested method. For lower lithium contents PBE fails to describe the *c* lattice parameter correctly, whereas with PBE and PBE + U ($U_{eff} = 3.5$ eV) including dispersion correction the deviations are less than 1 % independent of the dispersion correction scheme. The best agreement with the experimental structure of $LiTiS_2$ and TiS_2 is obtained using the PBE + U-D3 method with a maximum error of 3 %.

The band structure calculations for TiS_2 have shown that PBE does not provide a correct picture of the electronic properties of TiS_2 as it predicts a diamagnetic ground state. The same ground state is also obtained for Li_xTiS_2 for $x \ll 1$. PBE + U provides a band gap which is in good agreement with experimental data although the U parameter has not been optimized for this property. We expect that this method would provide a good account of the electronic properties of Li_xTiS_2 in the full range between 0 and 1.

NMR parameters calculated with PBE are also not satisfying in comparison to experimental data, in particular if the effects of Li content are considered. Absolute C_q values and trends with decreasing x obtained with PBE + U-D3 are in good agreement with experiment for both DM and FM states. At variance, only the chemical shift $\Delta\delta(^7\text{Li})$ calculated in the DM state is in agreement with available experimental data.

For Li ion migration in Li_xTiS_2 with $x \approx 1$, we have shown that only one migration pathway exists where the Li ion migrates via the tetrahedral position. The activation energy calculated with PBE + U-D3 in the diamagnetic state is 0.40 eV This is in good agreement with the experimental reference value Q_{max} of 0.48 eV. The activation energies obtained with the PBE based calculations (0.42, 0.45 eV) are much lower than previously calculated barriers at LDA level (0.7 eV) [16]. This is partly attributed to the well known overbinding of the LDA approach.

From the present results we conclude that both applied correction schemes, i.e. the dispersion correction and on-site Coulomb repulsion are important. Dispersion correction significantly improves the calculated structure parameters, in particular for $x \rightarrow 0$. The on-site Coulomb repulsion term U improves the calculated electronic properties and NMR parameters. The calculated electronic ground state at 0 K is ferromagnetic. However, a diamagnetic spin state should be used for the calculation of lattice parameter, NMR parameters and migration barriers, as experiments are mostly performed at room temperature at which Li_xTiS_2 shows diamagnetic state.

Acknowledgment: Support by the Deutsche Forschungsgemeinschaft (DFG) within the Research Unit 1277 (molife) and by Leibniz Universität IT Services (LUIS) is gratefully acknowledged. P. H. acknowledges personal funds within the program 'Top Seven' of the Faculty of Natural Sciences at Leibniz Universität Hannover.

References

1. K. Ozawa, Solid State Ion. **69** (1994) 212.
2. M. S. Whittingham, Science **192** (1976) 1126.
3. M. S. Whittingham, Prog. Solid State Ch. **12** (1978) 41.
4. A. H. Thompson, C. R. Symon, Solid State Ion. **3** (1981) 175.
5. C. Umrigar, D. E. Ellis, D.-S. Wang, H. Krakauer, M. Posternak, Phys. Rev. B **26** (1982) 4935.
6. R. Schöllhorn, A. Payer, Angew. Chem. **97** (1984) 57.
7. S. Sinha, D. W. Murphy, Solid State Ion. **20** (1986) 81.
8. M. Inoue, H. Hughes, A. Yoffe, Adv. Phys. **38** (1989) 565.
9. W. Küchler, P. Heitjans, A. Payer, R. Schöllhorn, Solid State Ion. **70** (1994) 434.

10. C. Prigge, W. Müller-Warmuth, R. Schöllhorn, Z. Phys. Chem. **189** (1995) 153.
11. Z. Y. Wu, F. Lemoigno, P. Gressier, G. Ouvrard, P. Moreau, J. Rouxel, C. R. Natoli, Phys. Rev. B **54** (1996) R11009.
12. D. G. Clerc, R. D. Poshusta, A. C. Hess, J. Phys. Chem. A **101** (1997) 8926.
13. L. Benco, J.-L. Barras, M. Atanasov, C. Daul, E. Deiss, J. Solid State Chem. **145** (1999) 503.
14. T. Bredow, P. Heitjans, M. Wilkening, Phys. Rev. B **70** (2004) 115111.
15. M. Wilkening, W. Küchler, P. Heitjans, Phys. Rev. Lett. **97** (2006) 065901.
16. A. Van der Ven, J. C. Thomas, Q. Xu, B. Swoboda, D. Morgan, Phys. Rev. B **78** (2008) 104306.
17. J. Bhattacharya, A. Van der Ven, Phys. Rev. B **83** (2011) 144302.
18. M. M. Islam, T. Bredow, Z. Phys. Chem. **226** (2012) 449.
19. S. Nakhal, M. Lerch, J. Koopman, M. M. Islam, T. Bredow, Z. Anorg. Allg. Chem. **639** (2013) 2822.
20. L. Bernard, W. Glaunsinger, P. Colombet, Solid State Ion. **17** (1985) 81.
21. R. H. Friend, A. D. Yoffe, Adv. Phys. **36** (1987) 1.
22. M. Wilkening, Ultralangsame Ionenbewegung in Festkörpern – NMR-spektroskopische Studien an Lithium-Ionenleitern, Ph.D. thesis, Leibniz Universität Hannover (published at Logos Verlag Berlin) (2005).
23. M. Wilkening, P. Heitjans, Defect Diffus. Forum **237–240** (2005) 1182.
24. P. Heitjans, A. Schirmer, S. Indris, in: P. Heitjans, J. Kärger (Eds.), Diffusion in Condensed Matter: Methods, Materials, Models, Springer, Berlin and New York (2005), p. 367.
25. P. Heitjans, S. Indris, M. Wilkening, Diffusion Fundamentals **2** (2005) 226.
26. M. Wilkening, P. Heitjans, Chem. Phys. Chem. **13** (2012) 53.
27. Y.-S. Kim, H.-J. Kim, Y.-A. Jeon, Y.-M. Kang, J. Phys. Chem. A **113** (2009) 1129.
28. V. L. Chevrier, S. P. Ong, R. Armiento, M. K. Y. Chan, G. Ceder, Phys. Rev. B **82** (2010) 075122.
29. B. Wang, S. Luo, D. G. Truhlar, J. Phys. Chem. B **120** (2016) 1437.
30. K. Berland, V. R. Cooper, K. Lee, E. Schröder, T. Thonhauser, P. Hyldgaard, B. I. Lundqvist, Rep. Prog. Phys. **78** (2015) 066501.
31. S. Grimme, J. Antony, S. Ehrlich, H. Krieg, J. Chem. Phys. **132** (2010) 154104.
32. S. Grimme, S. Ehrlich, L. Goerigk, J. Comp. Chem. **32** (2011) 1456.
33. A. Tkatchenko, M. Scheffler, Phys. Rev. Lett. **102** (2009) 073005.
34. S. L. Dudarev, G. A. Botton, S. Y. Savrasov, C. J. Humphreys, A. P. Sutton, Phys. Rev. B **57** (1998) 1505.
35. B. Xu, S. Meng, J. Power Sources **195** (2010) 4971.
36. S. P. Ong, V. L. Chevrier, G. Hautier, A. Jain, C. Moore, S. Kim, X. Ma, G. Ceder, Energy Environ. Sci. **4** (2011) 3680.
37. M. Nakayama, M. Kaneko, M. Wakihara, Phys. Chem. Chem. Phys. **14** (2012) 13963.
38. T. Jiang, M. L. Falk, Phys. Rev. B **85** (2012) 245111.
39. R. Kutteh, M. Avdeev, J. Phys. Chem. C **118** (2014) 11203.
40. G. Kresse, J. Hafner, Phys. Rev. B **47** (1993) 558.
41. G. Kresse, J. Hafner, Phys. Rev. B **49** (1994) 14251.
42. G. Kresse, J. Furthmüller, Comp. Mater. Sci. **6** (1996) 15.
43. G. Kresse, J. Furthmüller, Phys. Rev. B **54** (1996) 11169.
44. P. E. Blöchl, Phys. Rev. B **50** (1994) 17953.
45. G. Kresse, D. Joubert, Phys. Rev. B **59** (1999) 1758.
46. H. J. Monkhorst, J. D. Pack, Phys. Rev. B **13** (1976) 5188.
47. J. P. Perdew, K. Burke, M. Ernzerhof, Phys. Rev. Lett. **77** (1996) 3865.
48. J. P. Perdew, K. Burke, M. Ernzerhof, Phys. Rev. Lett. **78** (1997) 1396.

49. A. V. Krukau, O. A. Vydrov, A. F. Izmaylov, G. E. Scuseria, J. Chem. Phys. **125** (2006) 224106.
50. P. E. Blöchl, O. Jepsen, O. K. Andersen, Phys. Rev. B **49** (1994) 16223.
51. J. Paier, Catal. Lett. **146** (2016) 861.
52. G. Henkelman, H. Jónsson, J. Chem. Phys. **113** (2000) 9978.
53. G. Henkelman, B. P. Uberuaga, H. Jónsson, J. Chem. Phys. **113** (2000) 9901.
54. P. Heitjans, S. Indris, J. Phys. Condens. Mat. **15** (2003) R1257.
55. M. M. Islam, T. Bredow, P. Heitjans, J. Phys. Condens. Mat. **24** (2012) 203201.
56. M. Wilkening, P. Heitjans, Phys. Rev. B **77** (2008) 024311.
57. D. L. Greenaway, R. Nitsche, J. Phys. Chem. Solids **26** (1965) 1445.
58. A. R. Beal, J. C. Knights, W. Y. Liang, J. Phys. C Solid State **5** (1972) 3531.
59. F. R. Shepherd, P. M. Williams, J. Phys. C Solid State **7** (1974) 4416.
60. C. H. Chen, W. Fabian, F. C. Brown, K. C. Woo, B. Davies, B. DeLong, A. H. Thompson, Phys. Rev. B **21** (1980) 615.
61. C. A. Kukkonen, W. J. Kaiser, E. M. Logothetis, B. J. Blumenstock, P. A. Schroeder, S. P. Faile, R. Colella, J. Gambold, Phys. Rev. B **24** (1981) 1691.
62. J. J. Barry, H. P. Hughes, P. C. Klipstein, R. H. Friend, J. Phys. C Solid State **16** (1983) 393.
63. P. C. Klipstein, R. H. Friend, J. Phys. C Solid State **17** (1984) 2713.
64. W. Drube, I. Schafer, M. Skibowski, J. Phys. C Solid State **20** (1987) 4201.
65. C. Wang, L. Dotson, M. McKelvy, W. Glaunsinger, J. Phys. Chem. **99** (1995) 8216.
66. A. Zunger, A. J. Freeman, Phys. Rev. B **16** (1977) 906.
67. G. A. Benesh, A. M. Woolley, C. Umrigar, J. Phys. C Solid State **18** (1985) 1595.
68. D. G. Clerc, R. D. Poshusta, A. C. Hess, J. Phys. Chem. **100** (1996) 15735.
69. C. M. Fang, R. A. de Groot, C. Haas, Phys. Rev. B **56** (1997) 4455.
70. D. R. Allan, A. A. Kelsey, S. J. Clark, R. J. Angel, G. J. Ackland, Phys. Rev. B **57** (1998) 5106.
71. S. Sharma, T. Nautiyal, G. S. Singh, S. Auluck, P. Blaha, C. Ambrosch-Draxl, Phys. Rev. B **59** (1999) 14833.
72. Y.-B. Qiao, G.-H. Zhong, D. Li, J.-L. Wang, X.-Y. Qin, Z. Zeng, Chinese Phys. Lett. **24** (2007) 1050.
73. K. Sanchez, P. Palacios, P. Wahnon, Phys. Rev. B **78** (2008) 235121.
74. B. Liu, J. Yang, Y. Han, T. Hu, W. Ren, C. Liu, Y. Ma, C. Gao, J. Appl. Phys. **109** (2011) 053717.
75. M. S. Whittingham, F. R. Gamble, Mater. Res. Bull. **10** (1975) 363.
76. W. Küchler, Kernspinresonanz-Untersuchungen zur Diffusion von Li in der schichtstrukturierten und der kubischen Interkalationsverbindung Li_xTiS_2, Ph.D. thesis, Leibniz Universität Hannover (1992).
77. B. M. Meyer, N. Leifer, S. Sakamoto, S. G. Greenbaum, C. P. Grey, Electrochem. Solid St. **8** (2005) A145.